The Multidimensional Character of Nucleosynthesis in Core-Collapse Supernovae

68

W. Raphael Hix and J. Austin Harris

Abstract

Observations of supernovae and their remnants reveal highly aspherical distributions of the newly-formed elements that are the dying stars' contributions to the interstellar medium. Modern simulations of the supernova's neutrino-powered central engine reveal that these inhomogeneities originate in the first seconds of the explosions. Yet, much of our understanding of supernova nucleosynthesis is based on spherically symmetric models of the explosions. Recent simulations, combining high-fidelity treatments of the neutrino field that drives the explosion, the multidimensional fluid flow that taps this energy source, and the thermonuclear kinetics responsible for the composition of the ejecta, are revealing the limitations of our spherically symmetric understanding. Here, we highlight these recent results to presage the changes in our understanding of supernova nucleosynthesis that will result from a full appreciation of the multidimensional character of core-collapse supernovae.

Contents

W.R. Hix (✉)
Physics Division, Oak Ridge National Laboratory, Oak Ridge, TN, USA

Department of Physics and Astronomy, University of Tennessee, Knoxville, TN, USA
e-mail: raph@ornl.gov

J.A. Harris
Nuclear Science Division, Lawrence Berkeley National Laboratory, Berkeley, CA, USA
e-mail: austin@lbl.gov

A.W. Alsabti, P. Murdin (eds.), *Handbook of Supernovae*,
https://doi.org/10.1007/978-3-319-21846-5_77

1 Introduction

From observations of supernovae and supernova remnants, it is readily apparent that core-collapse supernovae (CCSNe) enrich their local environment with a rich mix of newly synthesized elements. For example, the detection of radioactive ^{57}Co, with a half-life of 272 days, in Supernova 1987A and ^{44}Ti, with a half-life of 60 years, in the Cassiopeia A supernova remnant is proof that recently created elements are released during the explosion. A myriad of supernova observations reveal the nuclear composition and distribution of the ejecta during the outburst (see, e.g., ▶ Chap. 31, "Spectra of Supernovae During the Photospheric Phase"). As discussed in ▶ Chap. 22, "Supernovae from Massive Stars", the beginning of the end of a massive star finds its core composed of iron, nickel, and similar elements, the products of nuclear statistical equilibrium (NSE), an equilibrium among the strong and electromagnetic nuclear reaction which favors the most bound nuclear species. This core is surrounded by concentric shells of successively lighter elements which recapitulate the sequence of nuclear burning that occurred in the core during the star's lifetime. A core-collapse supernova serves both to disperse the elements that were synthesized within the star during its lifetime and to synthesize and disperse new elements, providing an important link in our chain of origin from the Big Bang to the present. With a wide variety of nuclear fuels present in the progenitor star and a diversity of thermodynamic condition sampled by the ejecta, the deaths of massive stars are the dominant source of elements in the periodic table between oxygen and iron. These very elements are highlighted in observations of supernova remnants like Cassiopeia A, Puppis A, G292.0 + 1.8, and SN 1987A. Chapters ▶ 78, "X-Ray Emission Properties of Supernova Remnants" and ▶ 85, "Supernova Remnants as Clues to Their Progenitors" review the introduction of newly made elements into the interstellar medium in supernova remnants. There is also evidence from galactic chemical evolution that CCSNe, or one of the related deaths of massive stars (Oxygen-Neon core collapse, collapsar, etc.), are linked to the production of half the elements heavier than iron in the r-process. However, current CCSN simulations are hard pressed to confirm this (see ▶ Chap. 71, "Making the Heaviest Elements in a Rare Class of Supernovae").

These observations of supernova remnants further indicate that these newly made nuclei are being ejected in a geometrically complex, elementally inhomogeneous fashion. This consistent pattern of extensive, large-scale mixing of the chemical elements within the ejecta is also evident during the supernova itself. Mazzali et al. (2007) infer from observations that the type Ic supernova SN 2002ap had an oxygen-rich inner core with ^{56}Ni at higher velocity, a strong indication of large-scale overturn. The case is particularly persuasive for supernova SN 1987A . Observed asymmetries in iron lines are most easily explained by the concentration of

iron-peak elements into high-velocity "bullets" (Spyromilio et al. 1990). The *Bochum event*, the rapid development of fine structure in the H_α line from SN 1987A roughly 2 weeks after the explosion (Hanuschik et al. 1988), was interpreted by Utrobin et al. (1995) as an indication that a large ($\sim 10^{-3}\,M_\odot$) clump of nickel was ejected at high velocity ($\sim 4700\,\mathrm{km\,s^{-1}}$) into the far hemisphere of the supernova. Similarly, near-IR observations of He I lines arising roughly 2 months after explosion were interpreted by Fassia and Meikle (1999) as indications of dense clumps of nickel mixed into the hydrogen envelope of SN 1987A. Spectra of Supernovae during the Photospheric Phase and Spectra of Supernovae in the Nebular Phase discuss in detail the myriad of supernova observations that reveal its nuclear composition and distribution.

2 Modeling Multidimensional Neutrino-Driven Supernovae

Considerable effort, both in personpower and computational time, have been expended understanding how the transformation of the iron core of a massive star into a neutron star results in a shock wave that expels the stellar envelope and creates new elements (see ▸ Chap. 40, "Neutrino-Driven Explosions"). Progress in computing power has enabled improvements in the treatments of neutrino transport, hydrodynamics, gravity, and nuclear microphysics, all essential ingredients in the central engine that drive the supernova explosion. And yet, for much of the 40 years since Colgate and White (1966) first modeled supernovae, the most detailed supernova models in the world have failed to produce explosions that match the most basic supernova observation, an explosion energy near 1 Bethe ($B = 10^{44}$ J).

This has caused the modeling of core-collapse supernova nucleosynthesis to rely on parameterized models, mostly spherically symmetric (one-dimensional; 1D), which replace the inner workings of the supernova with a kinetic energy *piston* or a thermal energy *bomb*. (See ▸ Nucleosynthesis in Spherical Explosion Models of Core-Collapse Supernovae for recent progress on such models.) In such simulations, the explosion's energy, its delay time, and the *mass cut*, which separates the ejecta from matter destined to become part of the neutron star, are externally supplied parameters. Aufderheide et al. (1991) demonstrated that these two parameterizations are largely compatible, with the largest differences coming in the inner regions of the ejecta. Much of the innermost ejecta in these 1D models is composed of the products of *α-rich freeze-out*, where rapid cooling of the matter by expansion at relatively low density leaves a composition rich in α-particles in addition to the iron, nickel, and neighboring species that typify the normal freeze-out of nuclear statistical equilibrium (NSE) . Parameterized spherically symmetric models find that above the innermost regions, heated sufficiently that helium, iron, and nickel dominate the composition, the passage of the shock leaves a layer rich in the α isotopes; ^{40}Ca, ^{36}Ar, ^{32}S and ^{28}Si, the products of incomplete silicon burning. Above this is a layer of ^{16}O, in the outer portions of which, significant fractions of ^{20}Ne, ^{24}Mg, and ^{12}C are found. Finally comes the helium layer and hydrogen envelope, assuming they were not driven off as part of the stellar wind. It is the inner

region that can be most strongly affected by the details of the explosion mechanism (Fryer et al. 2008). In the case of the neutrino-reheating mechanism, these effects include interaction with the tremendous flux of neutrinos, the effects of the fluid instabilities fueled by the neutrino heating, and the temporal delay in achieving the explosion.

The interactions with the neutrino field are important because virtually all simulations utilizing spectral neutrino transport (e.g., Bruenn et al. 2016; Buras et al. 2006; Marek and Janka 2009; Rampp and Janka 2002) exhibit decreased neutronization. This increases the *electron fraction*, Y_e, the fraction of electrons (and protons) per nucleon, in the outer neutrino-reheating region as a result of these interactions, a feature which the parameterized bomb/piston models cannot replicate. Fröhlich et al. (2006a) and Pruet et al. (2005) have shown that nucleosynthesis from spectral, neutrino-driven explosions is qualitatively different in composition from both parameterized models and gray (mean energy) neutrino transport models, with the possibility of neutrino-driven flows to $Y_e > 0.5$ producing isotopes with mass number $A > 64$. This makes the innermost regions of CCSNe a candidate production site for light p-process nuclei via the *νp-process*. The spherically symmetric models of Fröhlich et al. (2006a,b) were explicitly neutrino driven with a self-consistent determination of the mass cut. These models (and the more recent models of Perego et al. 2015) rely on an artificial increase in neutrino heating to produce explosions, which otherwise do not occur in such one-dimensional (1D) models. Pruet et al. (2005) achieved similar results with key neutrino opacities modified to favor a stronger explosion (see Buras et al. 2006, for details of this model). Both Fröhlich et al. (2006a) and Pruet et al. (2005) successfully resolved the common problem of overproduction of neutron-rich nickel and iron isotopes in bomb/piston models and increased Ti, Sc, Cu, and Zn production, overcoming a shortcoming of previous models when compared to metal-poor stars. Recently, Perego et al. (2015) have demonstrated the ability to successfully reproduce ^{56}Ni yields in SN 1987A by retroactively extending the mass cut to include late-time fallback, but at the cost of underproducing ^{44}Ti – a direct consequence of the imposed spherical symmetry, since α-rich freeze-out occurs most strongly in the innermost ejecta in such stratified models. Ugliano et al. (2012) computed spherically symmetric supernova models for more than 100 progenitor stars using the "lightbulb" approximation, wherein the neutrino transport calculation in and around the newly formed, *proto-neutron star* is replaced with a prescribed neutrino luminosity.

Rather than the expanding chemically distinct spheres of ejecta that emerge from spherically symmetric models, the picture of a supernova that emerges from the observations is one of metal-rich shrapnel tearing though the envelope of the now deceased star. Such evidence for asymmetries in SN 1987A motivated the first multidimensional studies of the propagation of the supernova shock through the star. As a result, for two decades it has been known that Rayleigh-Taylor instabilities originate at the star's Si/O and (C+O)/He boundaries (Hachisu et al. 1990; Herant and Benz 1992; Kane et al. 2000; Müller et al. 1991; Nagataki et al. 1998); however these instabilities do not mix nickel to sufficiently high velocities to account for observations of Supernova 1987A (see McCray 1993,

and references therein) and other core-collapse supernovae. The implication is that gross asymmetries must be present in the core and be part of the central engine itself. This has motivated increasingly realistic simulations of the nascent supernova shock's propagation through the stellar envelope. Kifonidis et al. (2003, 2006) used a parameterized "neutrino lightbulb" to drive 2D explosions. These simulations showed significantly higher velocities than previous models (Hachisu et al. 1990; Herant and Benz 1992; Müller et al. 1991). Hammer et al. (2010) and Wongwathanarat et al. (2013) expanded these studies to three dimensions, starting from the asymmetric parameterized neutrino-driven explosions (with gray neutrino transport, see Scheck et al. 2006). The simulations of Hammer et al. (2010) show that in 3D, metal-rich clumps suffer much less deceleration at the compositional shell interfaces. This results in asymptotic velocities of metal-rich clumps that are twice or thrice those found in 2D models, better matching observations. Wongwathanarat et al. (2013) demonstrated a strong correlation between anisotropic production and distribution of heavy elements created by explosive burning behind the shock and the kick velocity of the neutron star. Late-time 3D supernova simulations by Ellinger et al. (2012) and Young et al. (2008), which extended a spherically symmetric initial explosion model, also reveal dense knots in the ejecta.

In fact, the existence of asymmetries, even in the pre-supernova core, has been known for some time (see ▶ Chap. 69, "Influence of Non-spherical Initial Stellar Structure on the Core-Collapse Supernova Mechanism"), though these asymmetries have generally not been followed through core collapse and bounce and into supernova explosions in a consistent fashion. However, Couch and Ott (2013) and Müller and Janka (2015) have shown that artificially imposed but physically reasonable asphericities in the pre-collapse progenitor can qualitatively alter the post-bounce evolution. Couch et al. (2015) have taken this a step further, completing the last few minutes of silicon shell burning in 3D before modeling the collapse and explosion of the star, also in 3D, with approximate neutrino transport.

For the nucleosynthesis, the impact of multidimensional fluid flow can be pivotal. The mass cut, formerly the spherical mass coordinate separating matter destined to rejoin the interstellar medium from the matter that will become trapped within the proto-neutron star, becomes an amorphous, potentially discontinuous, boundary. The ability in multidimensions for accretion onto the proto-neutron star to continue after the explosion has begun to grow radically alters the behavior of fallback, with some of the infalling matter joining the ejecta while some is accreted. Despite the fundamentally multidimensional nature of a supernova explosion from its earliest moments, relatively limited work has addressed the impact of multidimensional behavior on the nucleosynthesis. From the handful of investigation that have looked at multidimensional effects on the ejecta, we have learned that significant differences occur in the fraction of ejecta which experiences α-rich freeze-out (Maeda et al. 2002; Magkotsios et al. 2010; Nagataki et al. 1998) and that larger ejecta velocities are possible, characterized by metal-rich clumps (Ellinger et al. 2012; Hammer et al. 2010; Kitaura et al. 2006; Wongwathanarat et al. 2013, 2015). In the neutrino-reheating paradigm, neutrino interactions also directly affect the

matter as it passes near the proto-neutron star, fundamentally altering the chemical composition of the ejecta.

3 New Insights

The combination of a neutrino-driven explosion and multidimensional fluid flow by Pruet et al. (2005) hinted at the importance of departing from stratified 1D simulations. However, despite the profusion of exploding first-principle models with spectral neutrino transport in recent years, very little investigation of CCSN nucleosynthesis from these models has been conducted. This curious deficit can be partially attributed to the prolonged times the supernova models must be evolved in order to fully characterize the ejecta and, therefore, compute the nucleosynthesis. While the central engine plays its role in driving the explosion in perhaps 1–2 s and nucleosynthesis is largely complete within, at most, a few seconds thereafter, the spatial and velocity distribution of the newly made isotopes continues to develop over many minutes as the shock propagates through the rest of the star and matter falls back onto the proto-neutron star. Many CCSN models with complex neutrino transport are stopped less than half a second after the formation of the proto-neutron star, even before the final explosion energy is determined, much less the composition, and fate, of much of the ejecta. In contrast, 1D bomb or piston models, with their much lower computational cost, are routinely run to the surface of the star and well beyond. In fact, groups of tens or even hundreds of such models are prepared to serve as input for galactic chemical evolution, a task that is currently unimaginable for 3D CCSN models with realistic neutrino transport.

Another advantage of the bomb/piston models is that they routinely use extensive nuclear networks, with as many as 2000 species (Rauscher et al. 2002). In contrast, at best, self-consistent models of the CCSN central engine utilize an α-network (composed of 13 nuclear species of even and equal neutron and proton numbers from helium to nickel) while separately tracking the neutronization. To compute more complete nucleosynthesis, post-processing calculations are performed based on temperature, density, and neutrino exposure histories for individual mass elements from the supernova model. Performing post-processing nucleosynthesis calculations based on one-dimensional models is relatively straightforward, since most one-dimensional simulations are Lagrangian. Thus the needed temporal histories of temperature and density are simply those of the individual Lagrangian mass elements. However, in multidimensions, non-smooth fluid motions result in highly tangled Lagrangian grids. As a result, Eulerian hydrodynamics, where the discretization occurs in space rather than mass, is used to perform most multidimensional stellar astrophysics simulations. (The exceptions being calculations using Smoothed Particle Hydrodynamics methods.) Because Eulerian codes use spatial discretization, the Lagrangian thermodynamic histories that are a natural result in a Lagrangian code are unavailable. Instead passive tracer particles are commonly employed. The primary limitations in a post-processing approach are the accuracy

of the energy generation rate provided by the approximation included within the hydrodynamics as well as the underestimate of the effects of mixing.

Nucleosynthesis studies of electron-capture supernovae (ECSNe), which arise from the collapse of oxygen-neon cores in Super Asymptotic Giant Branch (AGB) stars, are more mature, as these explosions are triggered almost immediately and therefore complete more rapidly than in Fe-core SNe. Unlike all but the lightest of Fe-core SNe, successful explosions can be obtained for these stars even in 1D simulations (see Supernovae from Super AGB Stars (8–12 Msun)). Multidimensional investigations of ECSN by Janka et al. (2008) and Kitaura et al. (2006) revealed weak explosions ($\sim$0.1 B) and less than 0.02 $M_\odot$ of ejecta ($\lesssim 0.01\,M_\odot$ of ^{56}Ni). ECSN nucleosynthesis studies (Wanajo et al. 2009, 2011, 2013a,b) based on post-processing of tracer particles from these supernova simulations find only modest impact from multidimensional effects, which is unsurprising given the successful 1D explosions. In these axisymmetric simulations, the authors describe a small amount of neutron-rich matter being dredged up from near the proto-neutron star during the early stages of the explosion, a phenomenon not seen in similar 1D simulations. As a result, the models of Wanajo et al. (2011) are characterized by lower minimum values of Y_e, ultimately enhancing the production of As, Se, Br, Kr, Rb, Sr, and Y relative to that of spherically symmetric simulations, but leaving the ejected masses of nickel and other iron-group elements unaffected. However isotopic variations in these elements are seen, particularly the enhanced production of the trace, but interesting, species ^{48}Ca (Wanajo et al. 2013a) and ^{60}Fe (Wanajo et al. 2013b). Multidimensional Fe-core CCSN models also exhibit convective overturn near the outer proto-neutron star layers, potentially with even greater affect on the nucleosynthesis and, given the necessity of multidimensionality to engender these explosions, occurs merely as a subset of other multidimensional effects. Consequently, the lessons learned from ECSN nucleosynthesis studies, with respect to multidimensional effects, provide only modest insight into the CCSN problem.

Recently, Bruenn et al. (2016) published a set of four axisymmetric models using self-consistent spectral flux-limited diffusion neutrino transport for 12, 15, 20, and 25 $M_\odot$ progenitors from Woosley and Heger (2007). These models were run for times greater than 1 s after bounce, the longest elapsed times of any models of this sophistication, in an effort to achieve a saturated explosion energy. The three lower mass models achieved relatively saturated explosion energies (growth rates less than 0.2 B/s) near the observed values of $\sim$1 B, while the 25 $M_\odot$ model, with an explosion energy of 0.7 B, is still exhibiting strong growth in the explosion energy (more than 0.05 B in the final 100 ms) even 1.4 s after bounce. The long running times of these models also allows much more complete investigation of CCSN nucleosynthesis than is generally possible for such sophisticated models. Comprehensive analysis of the nucleosynthesis from these models is in preparation (Harris et al. 2016a), as well as an analysis of the uncertainties in post-processing nucleosynthesis based on tracer particles (Harris et al. 2016b). While there is some uncertainty in the degree to which the nucleosynthesis predictions of axisymmetric models will replicate three-dimensional models (and, ultimately, three-dimensional

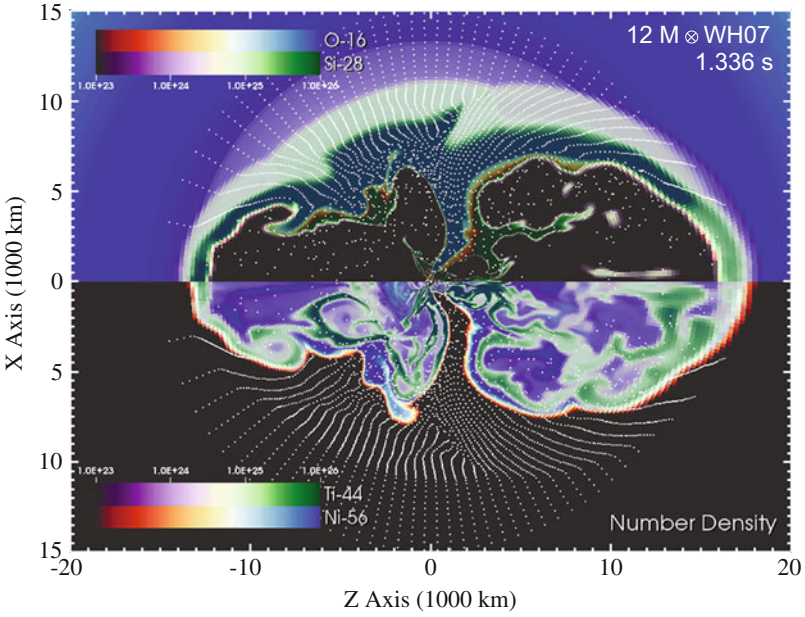

Fig. 1 Nucleosynthesis from an axisymmetric simulation of a core-collapse supernovae from a 12 $M_\odot$ star. The symmetry axis is horizontal at the center of the image. White dots denote the positions of tracer particles. Modified illustration originally published in Hix et al. (2014) (Published with permission of © W. R. Hix and collaborators, under the terms of the Creative Commons Attribution-NonCommercial-ShareAlike License)

reality), we present these results as a foreshadowing of the differences that the replacement of parameterized, spherically symmetric models with self-consistent multidimensional models can produce.

Figure 1 shows the spatial distribution of four distinct isotopes at the end of a two-dimensional simulation of the explosion of a 12 $M_\odot$ star, as computed by the small α-network that is used within the model. The progenitor was computed by Woosley and Heger (2007), who also computed a piston-driven parameterized supernova for the same star. The white dots mark the location of the tracer particles. The morphology of the nuclear products reflects the hydrodynamics of the model, which is dominated by two polar outflows and an equatorial accretion stream, potentially the consequence of the assumption of axisymmetry. The composition of the outflows is dominated by the products of α-rich freeze-out, portrayed here by ^{56}Ni and ^{44}Ti, while the equatorial regions are dominated by ^{28}Si and ^{16}O, partially burned matter from the progenitor's oxygen shell. The location of the supernova shock can be deduced by noting the deviation of these tracers from their originally radial distribution. From this, it is clear that the oblate shock has diverted the inflow of matter from polar latitudes toward the equator. The shape of the shock reveals that the velocity of the shock towards the poles is nearly twice that in the equatorial

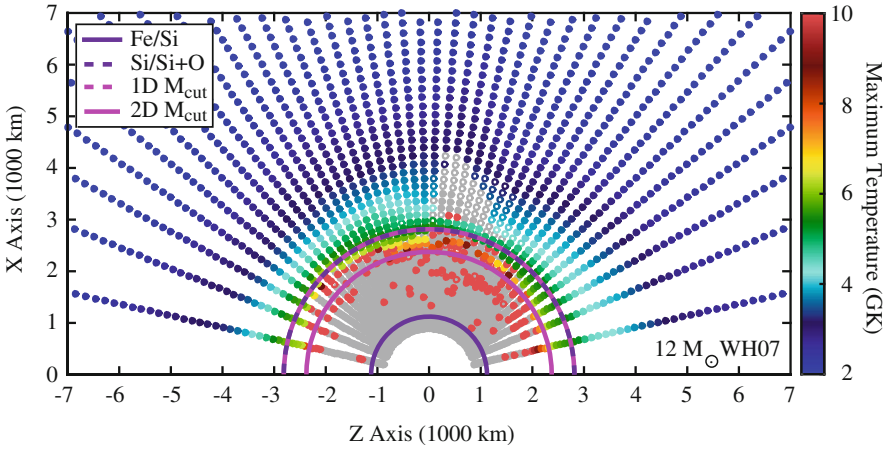

Fig. 2 Mapping the mass cut. The fate of mass elements 1.336 s after bounce as a function of their original location within the 12 $M_\odot$ progenitor star. Gray filled circles are matter within the neutron star, gray open circles represent matter bound to the neutron star. The colored circles are unbound matter, with the color representing the highest temperature reached by that parcel. Filled colored circles have positive radial velocity, open colored circles, though unbound, have negative radial velocity. Modified illustration originally published in Hix et al. (2014) (Published with permission of © W. R. Hix and collaborators, under the terms of the Creative Commons Attribution-NonCommercial-ShareAlike License)

regions. With the products of α-rich freeze-out moving outward more rapidly than the intermediate mass elements, we see a clear departure from the expectations of spherically symmetric models, where the stratification of elements is maintained by the explosion, causing the products of α-rich freeze-out to remain near the mass cut. Analysis detailed in Bruenn et al. (2016) indicates that at this point, it is silicon-rich matter that is continuing to accrete onto the proto-neutron star. While there remains the potential for the outflowing matter to be slowed and even stopped by continued hydrodynamic interaction, especially as the reverse shock forms as a result of the deceleration of the ejecta as it lifts the stellar envelope, it is the slower-moving intermediate mass elements that are more likely to be impacted.

Another clear departure from spherical symmetry can be seen in the fate of the parcels of matter. As Lagrangian elements, the paths of the tracer particles can be retraced to their origin in the progenitor. We can therefore map the mass cut in this multidimensional model in a way that is impossible from the Eulerian grid alone. Figure 2 is just such a map, for the same 12 $M_\odot$ model. In Fig. 2, the particles are placed at their original locations within the star, but color coded and shaped by their fate at the end of the simulation. Gray-colored particles are bound to the proto-neutron star, either already residing there (filled circles) or presently infalling toward the proto-neutron star (open circles). Colored particles are presently gravitationally unbound from the proto-neutron star, making them candidates for ejection, with the color indicating the peak temperature experienced by the particle, a proxy for

the nucleosynthesis processes that the particle has experienced. The filled colored circles are moving outward, having positive radial velocities. The open colored circles, while the sum of their kinetic, thermal, and gravitational potential energy are positive, are moving inward with negative radial velocities. Their ultimate fate must be considered uncertain. To provide context, the purple lines in Fig. 2 mark compositional interfaces in the progenitor star, the outer edges of the iron core (solid line), and the silicon shell (dotted line), where the composition transitions from more than 80 % silicon and sulfur, by mass, to predominately oxygen, with less than 10 % silicon. This silicon-oxygen interface, with a characteristic entropy of 4 k_B per baryon, is the location selected for the mass cut in the parameterized model of Woosley and Heger (2007), marked by the dashed pink line. For comparison, the solid pink line marks the spherical mass coordinate equal to the baryon mass of the proto-neutron star in this simulation, equivalent to the mass cut if this model had maintained spherical symmetry. The smaller radius of this "2D mass cut" indicates that the mass of the neutron star resulting from this 2D simulation is less than that of its 1D counterpart. Beyond this, there are clearly a significant number of ejecta particles below the 1D mass cut, colored red as an indication of the high temperatures they achieved as they plunged near the proto-neutron star before being swept into the ejecta. These parcels of matter began the simulation as part of the silicon shell and yet seem destined to be part of the ejecta. There are an equal number of gray particles above the solid pink line, including parts of the oxygen shell. The escape of part of the original silicon layer while part of the oxygen layer that started above it is captured by the proto-neutron star is a result quite against the intuition developed from spherically symmetric models. Our mental image of the mass cut clearly must be revised in view of the geometrically complex, disjoint nature of the ejecta revealed in multidimensional simulations. While there have been very few three-dimensional models of sufficient sophistication and sufficiently long enough elapsed time to explore the mass cut, those few do not suggest a return to sphericity in 3D (see, e.g., Ellinger et al. 2012).

The cumulative effects of the neutrino-driven, multidimensional fluid flows on the nucleosynthesis are highlighted in Fig. 3. Here the post-processing nucleosynthesis calculated by Harris et al. (2016a) for the 12 $M_\odot$ model of Bruenn et al. (2016) is compared to that of the parameterized explosion for the same progenitor calculated by Woosley and Heger (2007). Several general trends are visible, the results of the neutrino exposure and increased diversity of thermodynamic conditions that occur as a side effect of multidimensional fluid flow in these models. First, as is hinted at by the smaller radius of the 2D spherical mass cut in Fig. 2, more of the star is ejected in Bruenn et al. (2016) than in Woosley and Heger (2007), leading to a mild enhancement in the production of the dominant species from O through the intermediate mass elements. Second, as a result of the general increase in the proton richness of the ejecta that is bathed in the neutrino field, there is a significant increase (as large as two orders in magnitude) for production of species with $N \sim Z$ from S to Ni. Third, despite the general trend toward more proton-rich ejecta, there is also significant enhancement in the production of selected very neutron-rich species, for example, ^{48}Ca, ^{50}Ti, ^{54}Cr, ^{58}Fe, ^{64}Ni, ^{70}Zn, ^{76}Ge, and

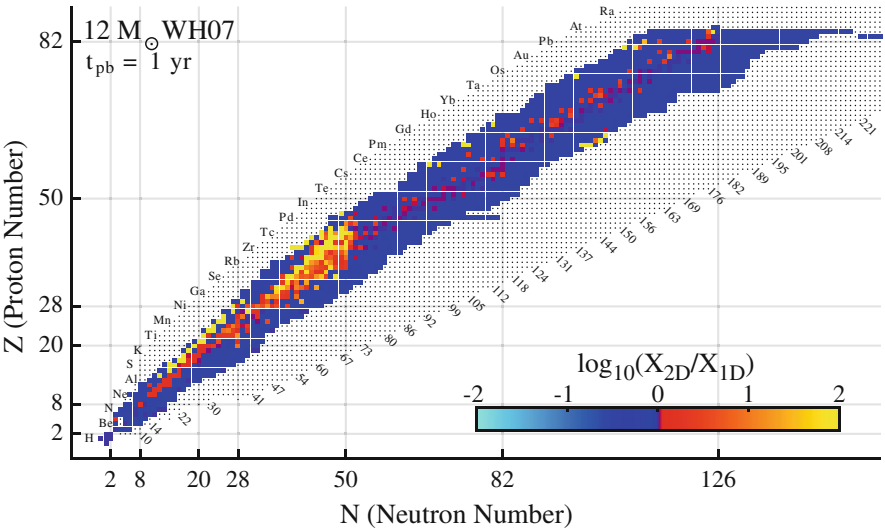

Fig. 3 The ratio of the composition as a function of proton and neutron numbers for the B12-WH07 model of Bruenn et al. (2016) to the parameterized model of Woosley and Heger (2007)

^{82}Se. These are produced in a small amount of matter that undergoes a neutron-rich ($Y_e < 0.45$), but α-poor, freeze-out from NSE in matter dredged up from the proto-neutron star, a mechanism similar to that discussed by Wanajo et al. (2013a) for ECSN. Finally, there is significant enhancement in the production of a wide range of species from $A = 60$ to $A = 90$, including the p-process species ^{88}Sr, ^{90}Zr, and ^{92}Mo. While production of these species in the proton-rich, neutrino-driven wind in the models of Fröhlich et al. (2006b) led to the discovery of the νp-process, that does not seem to be the cause here, as continued accretion onto the proto-neutron star has effectively suppressed the neutrino-driven wind to this point in the simulations, more than 1.3 s after bounce. Rather the production of these heavier species results from α-rich freeze-out in moderately neutron-rich matter ($0.45 < Y_e < 0.48$), more akin to the results of Woosley et al. (1994), but at lower entropies. Clearly, the wider range of thermodynamic conditions and neutrino exposures provided by these neutrino-driven, multidimensional models has far-ranging consequences for CCSN nucleosynthesis.

4 Limitations

While tracer particles are an essential tool for calculating realistic nucleosynthesis via post-processing for models, like those discussed in Sect. 3, that include only limited nucleosynthesis approximations self-consistently, they are not a panacea. As a passive, purely Lagrangian representation of the matter, they do not replicate the mixing that is seen in the gridded models. While the Eulerian grid overestimates

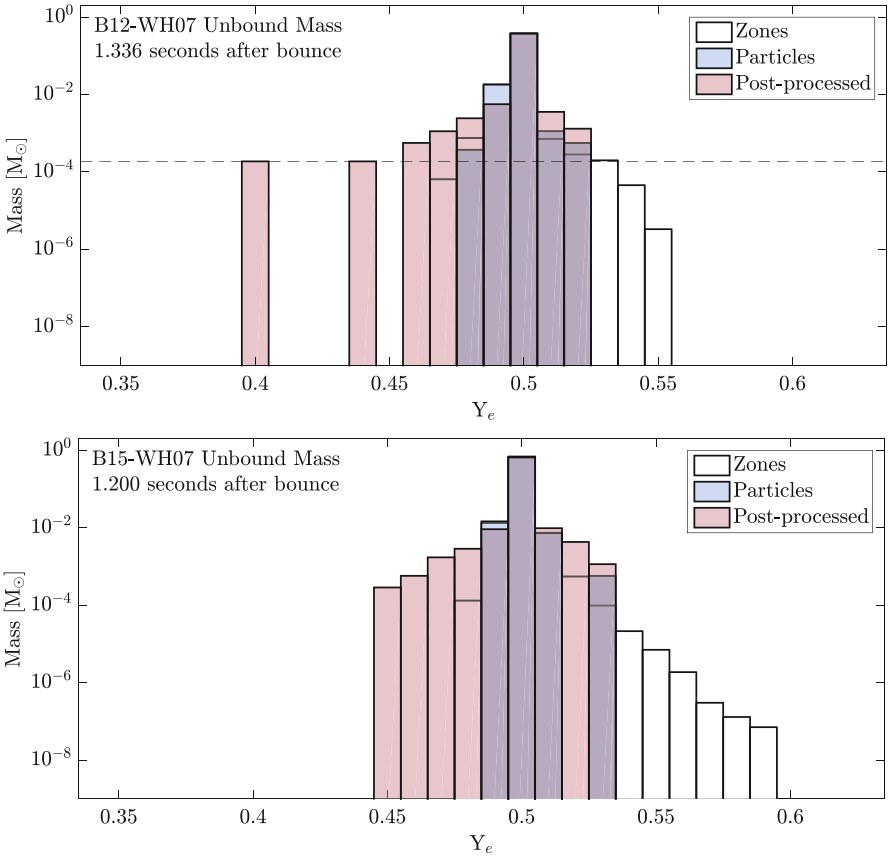

Fig. 4 The neutronization distribution of the unbound matter in a core-collapse supernovae simulations for 12 and 15 $M_\odot$ stars. The white histogram reflects the matter as described by the Eulerian computational grid. The *blue histogram* reflects the matter as described by the tracer particle position at the end of the simulation. The *red histogram* reflects the matter as described by the post-processing nucleosynthesis

the effects of mixing, assuming that macroscopic mixing, at the kilometer scale of the grid, is equivalent to microscopic mixing, at the scale of the collisional mean free path of the nuclei, the tracer particles ignore mixing completely. From the nucleosynthesis perspective, where only microscopic mixing impacts the reactive flow, reality will be intermediate between the course Eulerian view of the grid and the Lagrangian view of the tracers.

Figure 4 shows several interesting effects of the contrasting grids. The white blocks in Fig. 4 portray the distribution of electron fraction, Y_e, at the end of the simulation, as integrated over the Eulerian grid. The blue blocks portray the same integration over the tracer particles, using the Y_e values interpolated to the tracer particle positions from the Eulerian grid at the end of the simulation. The red blocks

display the electron fraction distribution as evolved by the post-processing nucleosynthesis calculation. For tracers that reach temperatures sufficient for nuclear statistical equilibrium (NSE) to be established, typically $\sim$6 GK for explosive conditions like those in CCSN, the value of Y_e, interpolated to the tracer position from the grid at the time when the particles temperature drops below the NSE threshold, is subsequently evolved within the nuclear reaction network. For tracers that never reach the NSE temperature threshold, the evolution within the reaction network follows from the initial value of Y_e. The post-processed distribution shows a much larger amount of neutron-rich ($Y_e < 0.5$) matter. Following these tracer's spatial evolution, we find matter which was swept into the ejecta from the vicinity of the proto-neutron star, similar to that found by Wanajo et al. (2009, 2011) for ECSN. In the CCSN case, as this matter is ejected at high speed from the central regions, it catches up with slower-moving ejecta above it and becomes mixed with that more neutron-poor ($Y_e \sim 0.5$) matter. Note that if the nucleosynthesis is complete before this (macroscopic) mixing occurs, which seems to be the case in this model, the result is a small admixture of neutron-rich nuclei within otherwise neutron-poor matter. In contrast, if the mixing occurs before the nucleosynthesis is complete, all trace of these neutron-rich species is removed. Correctly deducing the relative timing of the competing effects of compositional mixing and thermonuclear transmutation is a significant challenge for post-processing studies using tracer particles.

Another limitation of tracer particle-based post-processing is relatively poor resolution of this Lagrangian grid. In the simulations of Bruenn et al. (2016), which were launched in 2012, tracer masses of $\sim 10^{-4}\,M_\odot$ were used, a degree of tracer resolution similar to prior studies (Nagataki et al. 1997; Nishimura et al. 2006; Pruet et al. 2005). Subsequently, Nishimura et al. (2015) employed a tracer resolution $\sim$10 times higher in their study of the potential for the r-process in magnetically driven CCSN. The "medium" resolution case of Nishimura et al. (2015) is similar to Bruenn et al. (2016). Comparing the blue and white histograms in Fig. 4 reveals that the tracers, with their fixed mass resolution represented by the dashed lines in Fig. 4, are unable to resolve the most proton-rich ejecta. While this contribution is small in mass, it remains potentially interesting for the production of less abundant species (potentially including the νp-process). Even the highest resolution of Nishimura et al. (2015) would not be sufficient to resolve this material; an additional factor of 100 or more in the tracer resolution would be needed to trace the history of this material.

This incapability of the tracer particles to resolve the proton-rich wing of the distribution in Fig. 4 originates in the fixed mass of the particles and the challenge that creates on the tracer density in regions with low mass density. Effectively, the chances of a tracer sampling a high-density region are much larger than a neighboring low-density region. This has a direct impact on the nucleosynthesis, revealed in Fig. 5, because some of the most interesting nucleosynthesis process in CCSN occur in these high-entropy and relatively low-density regions. Beyond the failure to resolve the small amount of very proton-rich matter, this tracer resolution problem has other, larger consequences because the α-rich freeze-out is also a result

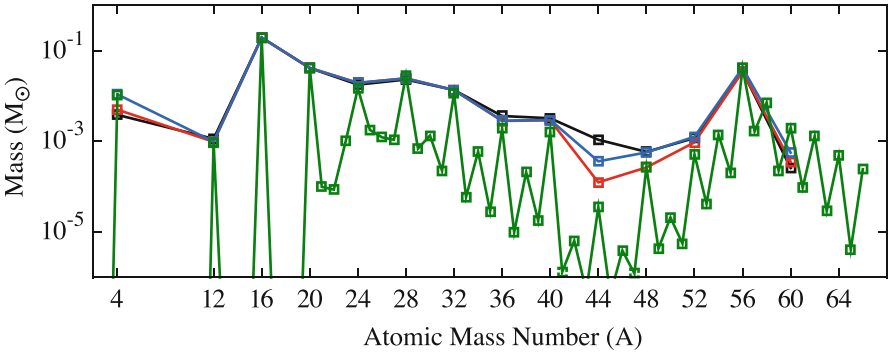

Fig. 5 The composition as a function of atomic mass for the B12-WH07 model of Bruenn et al. (2016). The *black line* displays the composition as computed by the α-network included within CHIMERA, the *red line* displays the composition computed with the same α-network in post-processing using tracer particle data. The blue line displays the composition when the transition from NSE to post-processing occurs at 8 GK, instead of ∼5.5 GK. The *green line* displays the composition computed in post-processing with a more realistic, 150 species, network (Modified illustration originally published in Harris et al. (2014), Published with permission of © J. A. Harris and collaborators, under the terms of the Creative Commons Attribution-NonCommercial-ShareAlike License)

of the ejection of high-entropy, low-density matter. Comparison of the black line in Fig. 5, the composition computed using the α-network built into the CCSN models of Bruenn et al. (2016), and the red line in Fig. 5, the composition calculated via post-processing using the same α-network and the same rules for transitioning matter from NSE into the network as are used within the model, reveals a significant under-prediction by the post-processing of the species that result from α-rich freeze-out. Most notable is ^{44}Ti, which differs by an order of magnitude, though ^{48}Cr and ^{52}Fe are also underproduced while ^{4}He and ^{60}Zn are slightly overproduced. Examination of Fig. 1 shows the relative paucity of tracer particles in the regions with large number densities of ^{44}Ti, providing visual confirmation of difficulty in resolving these low-density regions with Lagrangian particles.

The models of Bruenn et al. (2016) transition material into (or out of) NSE when the temperature in a zone rises above (drops below) ∼5.5 GK, an approach taken by many models of the CCSN central engine based on a comparison of the silicon burning timescale to the typical hydrodynamic timescale in the models. However, for the rapidly changing conditions in expanding CCSN matter, NSE has been shown to break down at higher temperatures (Hix and Thielemann 1999; Meyer et al. 1998). The assumption of NSE until ∼5.5 GK delays the onset of α-rich freeze-out and therefore limits its α richness. This is demonstrated in Fig. 5 by a comparison of the blue line, where the transition from NSE to post-processing with the α-network occurs at 8 GK, and red line, where this transition occurs at ∼5.5 GK. The abundances of ^{4}He, ^{44}Ti, ^{48}Cr, and ^{60}Zn are all enhanced by the earlier transition into the network, with ^{44}Ti increasing by a factor of 3.

Both of these effects, the tracer resolution and the NSE transition temperature, have their largest impact on ^{44}Ti, a species that is also well known to be overproduced by the α-network due to the nuclear flow from $A = 40$ to $A = 56$ occurring through reactions not included in the α-network. The extent of this over-prediction is illustrated by the green line in Fig. 5, which uses the same NSE transition as the blue line, but for a much more complete network of 150 species. Of course, the α-network neglects many of these 150 isotopes; thus, it cannot predict their abundances, though these tend to be less abundant species. Nevertheless, the α-network predictions for species from $A = 4$ up to $A = 32$, as well as $A = 56$, are in excellent agreement with the more realistic network. However, small discrepancies appear for $A = 36$ and $A = 40$ and overproduction as large as an order of magnitude plague the species from $A = 44$ to $A = 52$, while the production of species with $A > 56$ is suppressed. As we seek to make predictions of the production of these fruits of the α-rich freeze-out from our models, it is important to remember that the "positive" effects of improved NSE transition temperature and tracer resolutions are comparable to the more widely known "negative" impact of more realistic networks.

5 What Further Is Needed

While the iron-core-collapse investigations of Harris et al. (2016a,b) and the oxygen-neon-core-collapse investigations of Wanajo et al. (2013a,b), based on sophisticated neutrino radiation-hydrodynamic simulations, represent landmarks in our improving understanding of the nucleosynthesis that occurs in these supernovae, more work remains to be done on two fronts. First, while the sophisticated models on which Harris et al. (2016a,b) and Wanajo et al. (2013a,b) rely represent a tremendous improvement over purely hydrodynamic bomb/piston supernova models, this fidelity comes at tremendous computational cost. Especially if we wish to investigate sophisticated 3D CCSN models, we as a community can only afford a handful of models, compared to the hundreds of bomb or piston CCSN models that serve as input to galactic chemical evolution calculations. The hope would be, with the nucleosynthesis results from detailed 3D models in hand for comparison, models of intermediate complexity can be found that can reasonably replicate the nucleosynthesis of the more sophisticated models at a substantial savings in computational cost. Whether such a combination of limited neutrino transport approximation and dimensionality, the two principle drivers of computational cost for CCSN simulations, exists (or can be tuned) is an open question.

Second, as demonstrated in Sect. 4, the reliance on post-processing to address many of the species of interest in CCSN is a significant weakness. For the innermost supernova ejecta, the nuclear energy released by the recombination of α-particles into iron (and neighboring) nuclei ($\sim 10^{18}$ erg/g) is comparable to the change in the thermal energy of this gas due to expansion during the same time; thus, there is significant feedback between the rate of this nuclear recombination and the temperature evolution that is driving the recombination. The α-richness of the matter, and thus the abundance of species like ^{44}Ti, ^{57}Fe, ^{58}Ni,

and ^{60}Zn, therefore depends critically on this feedback. As a result, Magkotsios et al. (2010) found strong differences in the α-richness between different supernova models. In core-collapse supernovae, this α-rich freeze-out happens in the bath of neutrinos streaming from the core, fundamentally altering its neutronization, which in turn affects the path of the nuclear recombination. Clearly, supernova simulations which follow the composition with only an α-network are limited in their ability to calculate realistic nucleosynthesis, and these limitations cannot be completely redressed by post-processing with a more complete nuclear networks. A desire to better account for mixing of material while the nucleosynthesis is still underway further motivates the use of more complete nuclear networks within sophisticated neutrino radiation-hydrodynamic simulations. Finally, the much finer mass resolution of the Eulerian grid for the low-density regions, where the α-rich freeze-out occurs, favors replacing post-processing with a realistic network included within the supernova model. While the use of larger networks, with 150–200 species to capture the energetically significant reaction processes, adds significantly to the computational cost, the added cost is comparable to the cost of the neutrino transport calculations already performed. Thus the total cost is a small multiple of the cost of current models, making the use of moderate-sized networks an achievable goal in the near future. We have axisymmetric test simulations underway, which we hope to present within a year or two, and the rest of the community is likely to follow.

6 Conclusions

The near future will see great strides toward incorporating the lessons learned over the past two decades about the nature of the central core-collapse supernova engine into our modeling of the nucleosynthesis of these extraordinary events. Progress may be slow at first, as we build our database of these very expensive simulations and seek lesser approximations that still capture the essential impact of the neutrino-driven, multidimensional nature of the core-collapse supernova's central engine. Nonetheless, we can, within this decade, anticipate an improved understanding of the means by which a dying massive star is transformed into the nuclear seed stocks for the next generation of stars and planets, an understanding that finally takes into full account the myriad of physics that contributes to these spectacular explosions.

7 Cross-References

- ▸ Electron Capture Supernovae from Super Asymptotic Giant Branch Stars
- ▸ Making the Heaviest Elements in a Rare Class of Supernovae
- ▸ Neutrino-Driven Explosions
- ▸ Nucleosynthesis in Spherical Explosion Models of Core-Collapse Supernovae
- ▸ Spectra of Supernovae During the Photospheric Phase
- ▸ Spectra of Supernovae in the Nebular Phase

▶ Supernovae from Massive Stars
▶ Supernova Remnants as Clues to Their Progenitors
▶ X-Ray Emission Properties of Supernova Remnants

Acknowledgements This research was supported by the US Department of Energy Office of Nuclear Physics, the NASA Astrophysics Theory Program (NNH11AQ72I), and the National Science Foundation Theoretical Physics Program (PHY-1516197). The simulations here were performed via NSF TeraGrid resources provided by the National Institute for Computational Sciences under grant number TG-MCA08X010 and resources of the National Energy Research Scientific Computing Center.

References

Aufderheide MB, Baron E, Thielemann FK (1991) Shock waves and nucleosynthesis in type II supernovae. ApJ 370:630–642

Bruenn SW, Lentz EJ, Hix WR, Mezzacappa A, Harris JA, Messer OEB, Endeve E, Blondin JM, Chertkow MA, Marronetti P (2016) Chimera: a massively parallel, multi-physics code for core-collapse supernova simulations. ApJ 818:123

Buras R, Rampp M, Janka HT, Kifonidis K (2006) Two-dimensional hydrodynamic core-collapse supernova simulations with spectral neutrino transport. I. Numerical method and results for a 15 $M_{\odot}$ star. A&A 447:1049–1092. doi:10.1051/0004-6361:20053783, astro-ph/0507135

Colgate SA, White RH (1966) The hydrodynamic behavior of supernovae explosions. ApJ 143:626

Couch SM, Ott CD (2013) Revival of the Stalled Core-collapse supernova shock triggered by precollapse asphericity in the progenitor star. ApJ 778:L7. doi:10.1088/2041-8205/778/1/L7, 1309.2632

Couch SM, Chatzopoulos E, Arnett WD, Timmes FX (2015) The Three-dimensional evolution to core collapse of a massive star. ApJ 808:L21. doi:10.1088/2041-8205/808/1/L21, 1503.02199

Elekes Z, Fulop Z, Gyurky G, Kertesz Z, Kiss G. G, Simon A, Somorjai E, Torok Z, Frei Z, Vinko J, Keresturi A & Szabo R (eds) (2014) Proceedings of nuclei in the Cosmos XIII, SISSA Proceedings of Science

Ellinger CI, Young PA, Fryer CL, Rockefeller G (2012) A case study of small-scale structure formation in three-dimensional supernova simulations. ApJ 755:160. doi:10.1088/0004-637X/755/2/160, 1206.1834

Fassia A, Meikle WPS (1999) ^{56}Ni dredge-up in Supernova 1987A. MNRAS 302:314–320. doi:10.1046/j.1365-8711.1999.02127.x, astro-ph/9809244

Fröhlich C, Hauser P, Liebendörfer M, Martínez-Pinedo G, Thielemann FK, Bravo E, Zinner NT, Hix WR, Langanke K, Mezzacappa A, Nomoto K (2006a) Composition of the innermost supernova ejecta. ApJ 637:415–426. doi:10.1086/498224, astro-ph/0410208

Fröhlich C, Martínez-Pinedo G, Liebendörfer M, Thielemann FK, Bravo E, Hix WR, Langanke K, Zinner NT (2006b) Neutrino-induced nucleosynthesis of A> 64 nuclei: the nu p-process. Phys Rev Lett 96(14):142502. doi:10.1103/PhysRevLett.96.142502, astro-ph/0511376

Fryer C, Young P, Bennet ME, Diehl S, Herwig F, Hirschi R, Hungerford A, Pignatari M, Magkotsios G, Rockefeller G, Timmes FX (2008) Nucleosynthesis from supernovae as a function of explosion energy from NuGrid. In: Schatz H, Austin S, Beers T, Brown A, Brown E, Cyburt R, Lynch W, Zegers R (eds) Proceedings of nuclei in the cosmos X, SISSA proceedings of science, p 101

Hachisu I, Matsuda T, Nomoto K, Shigeyama T (1990) Nonlinear growth of Rayleigh-Taylor instabilities and mixing in SN 1987A. ApJ 358:L57–LL61

Hammer NJ, Janka HT, Müller E (2010) Three-dimensional simulations of mixing instabilities in supernova explosions. ApJ 714:1371–1385. doi:10.1088/0004-637X/714/2/1371, 0908.3474

Hanuschik RW, Thimm G, Dachs J (1988) H-alpha fine-structure in SN 1987A within the first 111 days. MNRAS 234:41P–49P

Harris JA, Hix WR, Chertkow MA, Bruenn SW, Lentz EJ, Messer OEB, Mezzacappa A, Blondin JM, Marronetti P, Yakunin KN (2014) Advancing nucleosynthesis in self-consistent, multidimensional models of core-collapse supernovae. In: Elekes Z et al (eds) Proceedings of nuclei in the Cosmos XIII, SISSA Proceedings of Science, PoS(NIC XIII)099, 1411.0037

Harris JA, Hix WR, Chertkow MA, Bruenn SW, Lentz EJ, Messer OEB, Mezzacappa A, Blondin JM, Endeve E, Lingerfelt EJ, Marronetti P, Yakunin KN (2016a, in preparation) The nucleosynthesis of axisymmetric Ab initio core-collapse supernova simulations of 12–25 $M_{\odot}$ Stars. ApJ

Harris JA, Hix WR, Chertkow MA, Lee CT, Lentz EJ, Messer OEB (2016b, in preparation) Implications for post-processing nucleosynthesis of core-collapse supernova models with lagrangian particles. ApJ

Herant M, Benz W (1992) Postexplosion hydrodynamics of SN 1987A. ApJ 387: 294–308

Hix WR, Thielemann FK (1999) Silicon burning II: Quasi-Equilibrium and explosive burning. ApJ 511:862–875

Hix WR, Harris JA, Lentz EJ, Bruenn SW, Chertkow MA, Messer OEB, Mezzacappa A, Blondin JM, Endeve E, Marronetti P, Yakunin KN (2014) Multidimensional simulations of core-collapse supernovae and the implications for nucleosynthesis. In: Elekes Z, et al (eds) Proceedings of nuclei in the Cosmos XIII, SISSA Proceedings of Science, p PoS(NIC XIII)019

Janka HT, Müller B, Kitaura FS, Buras R (2008) Dynamics of shock propagation and nucleosynthesis conditions in O-Ne-Mg core supernovae. A&A 485:199–208. doi:10.1051/0004-6361:20079334, 0712.4237

Kane J, Arnett D, Remington BA, Glendinning SG, Bazán G, Müller E, Fryxell BA, Teyssier R (2000) Two-dimensional versus three-dimensional supernova hydrodynamic instability growth. ApJ 528:989–994

Kifonidis K, Plewa T, Janka HT, Müller E (2003) Non-spherical core collapse supernovae. I. Neutrino-driven convection, Rayleigh-Taylor instabilities, and the formation and propagation of metal clumps. A&A 408:621–649

Kifonidis K, Plewa T, Scheck L, Janka HT, Müller E (2006) Non-spherical core collapse supernovae. II. The late-time evolution of globally anisotropic neutrino-driven explosions and their implications for SN 1987 A. A&A 453:661–678. doi:10.1051/0004-6361:20054512, astro-ph/0511369

Kitaura FS, Janka HT, Hillebrandt W (2006) Explosions of O-Ne-Mg cores, the Crab supernova, and subluminous type II-P supernovae. A&A 450:345–350. doi:10.1051/0004-6361:20054703, astro-ph/0512065

Maeda K, Nakamura T, Nomoto K, Mazzali PA, Patat F, Hachisu I (2002) Explosive nucleosynthesis in aspherical hypernova explosions and late-time spectra of SN 1998bw. ApJ 565:405–412

Magkotsios G, Timmes FX, Hungerford AL, Fryer CL, Young PA, Wiescher M (2010) Trends in ^{44}Ti and ^{56}Ni from core-collapse supernovae. ApJS 191:66–95. doi:10.1088/0067-0049/191/1/66, 1009.3175

Marek A, Janka HT (2009) Delayed neutrino-driven supernova explosions aided by the standing accretion-shock instability. ApJ 694:664–696. doi:10.1088/0004-637X/694/1/664, 0708.3372

Mazzali PA, Kawabata KS, Maeda K, Foley RJ, Nomoto K, Deng J, Suzuki T, Iye M, Kashikawa N, Ohyama Y, Filippenko AV, Qiu Y, Wei J (2007) The aspherical properties of the energetic type Ic SN 2002ap as inferred from its nebular spectra. ApJ 670:592–599. doi:10.1086/521873, 0708.0966

McCray R (1993) Supernova 1987A revisited. ARA&A 31:175–216

Meyer BS, Krishnan TD, Clayton DD (1998) Theory of Quasi-Equilibrium nucleosynthesis and applications to matter expanding from high temperature and density. ApJ 498:808

Müller B, Janka HT (2015) Non-radial instabilities and progenitor asphericities in core-collapse supernovae. MNRAS 448:2141–2174. doi:10.1093/mnras/stv101, 1409.4783

Müller E, Fryxell B, Arnett D (1991) Instability and clumping in SN 1987A. A&A 251:505–514

Nagataki S, Hashimoto M, Sato K, Yamada S (1997) Explosive nucleosynthesis in axisymmetrically deformed type II supernovae. ApJ 486:1026

Nagataki S, Shimizu TM, Sato K (1998) Matter mixing from axisymmetric supernova explosion. ApJ 495:413. doi:10.1086/305258, astro-ph/9709152

Nishimura N, Takiwaki T, Thielemann FK (2015) The r-process nucleosynthesis in the various Jet-like explosions of magnetorotational core-collapse supernovae. ApJ 810:109. doi:10.1088/0004-637X/810/2/109, 1501.06567

Nishimura S, Kotake K, Hashimoto Ma, Yamada S, Nishimura N, Fujimoto S, Sato K (2006) r-Process nucleosynthesis in magnetohydrodynamic jet explosions of core-Collapse supernovae. ApJ 642:410–419. doi:10.1086/500786, astro-ph/0504100

Perego A, Hempel M, Fröhlich C, Ebinger K, Eichler M, Casanova J, Liebendörfer M, Thielemann FK (2015) PUSHing core-collapse supernovae to explosions in spherical symmetry I: the model and the case of SN 1987A. ApJ 806:275. doi:10.1088/0004-637X/806/2/275, 1501.02845

Pruet J, Woosley SE, Buras R, Janka HT, Hoffman RD (2005) Nucleosynthesis in the hot convective bubble in core-collapse supernovae. ApJ 623:325–336

Rampp M, Janka HT (2002) Radiation hydrodynamics with neutrinos. Variable eddington factor method for core-collapse supernova simulations. A&A 396:361–392

Rauscher T, Heger A, Hoffman RD, Woosley SE (2002) Nucleosynthesis in massive stars with improved nuclear and stellar physics. ApJ 576:323–348

Schatz H, Austin S, Beers T, Brown A, Brown E, Cyburt R, Lynch W, Zegers R (eds) Proceedings of nuclei in the cosmos X, SISSA proceedings of science

Scheck L, Kifonidis K, Janka HT, Müller E (2006) Multidimensional supernova simulations with approximative neutrino transport. I. Neutron star kicks and the anisotropy of neutrino-driven explosions in two spatial dimensions. A&A 457:963–986. doi:10.1051/0004-6361:20064855

Spyromilio J, Meikle WPS, Allen DA (1990) Spectral line profiles of iron and nickel in supernova 1987A - Evidence for a fragmented nickel bubble. MNRAS 242:669–673

Ugliano M, Janka HT, Marek A, Arcones A (2012) Progenitor-explosion connection and remnant birth masses for neutrino-driven supernovae of iron-core progenitors. ApJ 757:69. doi:10.1088/0004-637X/757/1/69, 1205.3657

Utrobin VP, Chugai NN, Andronova AA (1995) Asymmetry of SN 1987A: Fast Ni-56 clump. A&A 295:129–135

Wanajo S, Nomoto K, Janka HT, Kitaura FS, Müller B (2009) Nucleosynthesis in electron capture supernovae of asymptotic giant branch stars. ApJ 695:208–220, doi:10.1088/0004-637X/695/1/208, 0810.3999

Wanajo S, Janka HT, Müller B (2011) Electron-capture Supernovae as the origin of elements beyond iron. ApJ 726:L15, doi:10.1088/2041-8205/726/2/L15, 1009.1000

Wanajo S, Janka HT, Müller B (2013a) Electron-capture Supernovae as origin of ^{48}Ca. ApJ 767:L26, doi:10.1088/2041-8205/767/2/L26, 1302.0929

Wanajo S, Janka HT, Müller B (2013b) Electron-capture Supernovae as Sources of ^{60}Fe. ApJ 774:L6, doi:10.1088/2041-8205/774/1/L6, 1307.3319

Wongwathanarat A, Janka HT, Müller E (2013) Three-dimensional neutrino-driven supernovae: Neutron star kicks, spins, and asymmetric ejection of nucleosynthesis products. A&A 552:A126, doi:10.1051/0004-6361/201220636, 1210.8148

Wongwathanarat A, Müller E, Janka HT (2015) Three-dimensional simulations of core-collapse supernovae: from shock revival to shock breakout. A&A 577:A48, doi:10.1051/0004-6361/201425025, 1409.5431

Woosley SE, Heger A (2007) Nucleosynthesis and remnants in massive stars of solar metallicity. Phys Rep 442:269–283, doi:10.1016/j.physrep.2007.02.009, astro-ph/0702176

Woosley SE, Wilson JR, Mathews GJ, Hoffman RD, Meyer BS (1994) The r-process and neutrino-heated supernova ejecta. ApJ 433:229–246

Young P, Ellinger C, Arnett D, Fryer C, Rockefeller G (2008) Spatial distribution of nucleosynthesis products in Cassiopeia A: comparison between observations and 3D explosion models. In: Schatz H, Austin S, Beers T, Brown A, Brown E, Cyburt R, Lynch W, Zegers R (eds) Proceedings of nuclei in the cosmos X, SISSA proceedings of science, p 20. 0811.4655